

## Magnetic structure of $\text{UNi}_2\text{Si}_2$

H. Lin

*Department of Physics, McMaster University, Hamilton, Ontario, Canada L8S 4M1*

L. Rebelsky

*Department of Physics, Brookhaven National Laboratory, Upton, New York 11973*

M. F. Collins and J. D. Garrett

*Institute for Materials Research, McMaster University, Hamilton, Ontario, Canada L8S 4M1*

W. J. L. Buyers

*AECL Research, Chalk River Laboratories, Chalk River, Ontario, Canada K0J 1J0*

(Received 28 November 1990)

The magnetic ordering and phase transitions have been studied in  $\text{UNi}_2\text{Si}_2$  single crystals by neutron diffraction. Three distinct ordered phases are observed, all with magnetic moments along the  $c$  axis. The high-temperature ( $103 < T < 124$  K) phase is an incommensurate longitudinal spin-density wave with temperature-dependent wave vector. At 110 K,  $\mathbf{q} = (0, 0, 0.745 \pm 0.002)$ . The intermediate temperature ( $53 < T < 103$  K) phase is a simple body-centered antiferromagnet with a moment of  $(1.6 \pm 0.3)\mu_B$ . The low-temperature phase shows a similar scattering pattern to that of the high-temperature phase with  $\mathbf{q} = (0, 0, \frac{2}{3})$ , and with extra scattering at the nuclear Bragg peaks corresponding to a ferromagnetic moment  $\mu_z$  of  $(1.0 \pm 0.3)\mu_B$  per uranium atom. This pattern can be interpreted either as a longitudinal spin-density wave with maximum moment  $\mu_0 = (2.7 \pm 0.3)\mu_B$  and a ferromagnetic component or as a squared-up wave with uranium moments of  $2.22\mu_B$ , two thirds of which are along  $+z$  and one third along  $-z$ . Hysteresis is observed in the low-temperature phase transition. The phase transitions at 53 and 103 K are both first order. At  $124 \pm 1$  K there is a critical phase transition to the paramagnetic state with  $\beta = 0.35 \pm 0.03$ . Above 124 K conventional critical scattering is observed centered on the wave vector  $\mathbf{q}$ .

### I. INTRODUCTION

There is a great interest in the class of materials  $\text{UT}_2\text{Si}_2$  ( $T$ =transition metal). Although most compounds crystallize in the tetragonal  $\text{ThCr}_2\text{Si}_2$  structure, they show different kinds of magnetic ordering, heavy-fermion behavior, superconductivity, and enhanced Pauli paramagnetism.<sup>1</sup>

The first neutron-diffraction investigation of the magnetic ordering of  $\text{UNi}_2\text{Si}_2$  on a polycrystalline sample was performed by Chelmicki, Leciejewicz, and Zygmunt.<sup>2</sup> The experiment revealed a magnetic phase transition from a longitudinal spin-density-wave- (LSDW-) type structure to a collinear simple antiferromagnetism type at around 53 K and a Néel temperature at 103 K. Contrary to this result, magnetization measurements<sup>3,4</sup> show ferromagnetic ordering below 98 K and no phase transition at 53 K.

In this paper we show by neutron diffraction on single crystals that there is a third, hitherto unsuspected, incommensurate magnetic phase above 103 K. In addition, we determine the magnetic structure of all three phases and show that the ferromagnetism is in fact coexistent with a commensurate LSDW in the lowest-temperature phase.

### II. EXPERIMENTAL TECHNIQUES

The measurements were performed on two single crystals grown by a modified triple-arc Czochralski method.<sup>5</sup> Sample No. 1 is 15 mm long with a diameter of 7 mm; sample No. 2 is 40 mm long with a diameter of 6 mm. Both samples showed sharp single-crystal peaks with some minor asymmetric structure in the wings of the Bragg peaks. Sample No. 1 was in fact found to consist of two large single crystals widely separated in orientation. The earlier measurements were made on one of the two crystals in sample No. 1. Later, we repeated the measurements on sample No. 2, which did not contain a second crystal. Our measurements confirm the chemical crystal structure given in Ref. 2 at all temperatures from 11 K to room temperature. The lattice parameters are  $a = 3.958 \text{ \AA}$  and  $c = 9.514 \text{ \AA}$ , and  $a = 3.952 \text{ \AA}$  and  $c = 9.514 \text{ \AA}$  at 11 K for samples Nos. 1 and 2, respectively. The magnetic structure is, however, more complex than revealed by the powder data of Ref. 2.

Neutron-diffraction measurements were carried out on the N5 triple-axis spectrometer at the NRU reactor of Chalk River Laboratories. The samples were aligned with the  $(h0l)$  plane horizontal and mounted in a Displex refrigerator. The temperature range of the measurements

was 10–150 K, controlled to better than 0.1 K. An incident neutron wavelength of 2.37 Å was used in conjunction with a pyrolytic graphite filter in the scattered beam. For the experiment on sample No. 1, a silicon (111) reflection and a pyrolytic graphite (002) reflection were used as monochromator and analyzer, respectively, with collimation of 0.7° and 0.8° before and after the sample. For the experiment on sample No. 2, a silicon (111) reflection was used as both monochromator and analyzer with collimation of 0.55° and 0.6° before and after the sample.

### III. EXPERIMENTAL RESULTS AND ANALYSIS OF THE DATA

UNi<sub>2</sub>Si<sub>2</sub> has the tetragonal ThCr<sub>2</sub>Si<sub>2</sub> crystal structure with space group  $I4/mmm(D_{4h}^{17})$ . The arrangement of the atoms in a unit cell is as shown in Fig. 1. The uranium atoms occupy the  $2a$  position to form a simple body-centered tetragonal (bct) sublattice. The nickel atoms are in the  $4d$  positions and the silicon atoms in the  $4e$  positions. The Bragg reflections of the nuclear unit cell are of the form  $h+k+l=2n$ .

#### A. Magnetic ordering

A series of scans were taken along different directions in reciprocal space at fixed temperatures. Figure 2 shows the diffraction pattern for four such scans from sample No. 1 along the  $[10l]$  direction. In the paramagnetic state at 148 K, just the weak nuclear peak (101) is seen. At each of the lower temperatures shown, 110, 79, and 11 K, there are extra peaks in the pattern. These are the

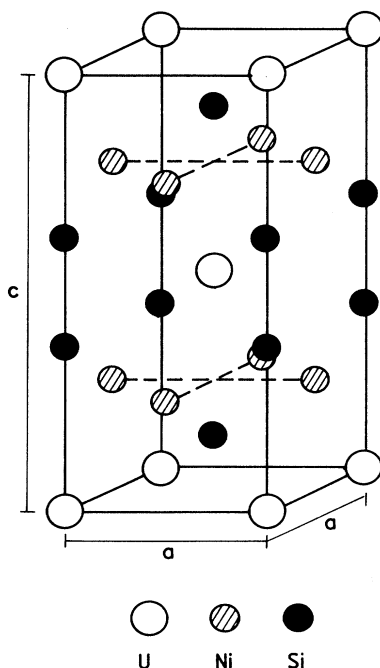


FIG. 1. Body-centered tetragonal crystal structure of UNi<sub>2</sub>Si<sub>2</sub>.

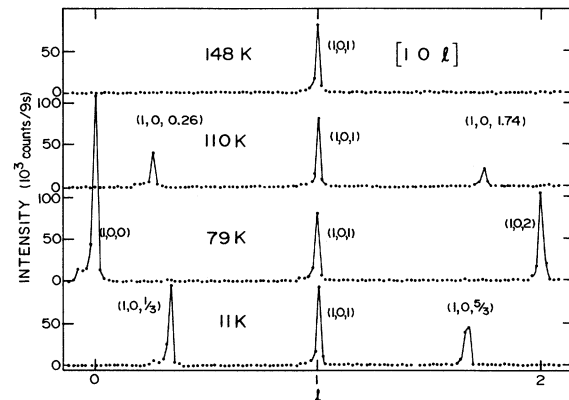


FIG. 2. Scans along the  $[10l]$  direction at 148, 110, 79, and 11 K.

magnetic Bragg peaks, and their different nature at the three temperatures indicates the presence of three distinct magnetic phases. As will be shown later, these phases are stable between 124 and 103 K, 103 and 53 K, and below 53 K. They will be called the high-, intermediate-, and low-temperature phases.

The asymmetric mosaic of the Bragg peaks of sample No. 1 is apparent from close inspection of Fig. 2; each Bragg peak has some minor structure on its left-hand side. The shape and width of all the magnetic Bragg peaks is the same as that of the nuclear peaks, indicating that in every case the magnetic peaks are sharp to within the experimental resolution.

#### B. High-temperature phase

A survey of the  $(h0l)$  plane indicates that this phase contains magnetic Bragg peaks of type  $(h,0,l\pm q_z)$  with  $h+l=2n$  and  $h\neq 0$ , where  $h$ ,  $l$ , and  $n$  are integers. We have observed all of the ten Bragg peaks of this type nearest to the origin, and these account for all the differences between the diffraction pattern at 110 K and that at 148 K. Least-squares fitting to the position of these peaks gives  $q_z=0.745\pm 0.002$ .

A diffraction pattern of this type corresponds to a spin-density wave with wave vector  $\mathbf{q}=(0,0,q_z)$ . The restriction  $h\neq 0$  indicates that the moments are aligned along the  $c$  direction so that the spin density wave is longitudinal. In our description of the spin-density wave, we will make the assumption that only the uranium atoms carry magnetic moment.<sup>2,6</sup> There is nothing in our data that requires the presence of a nickel moment for its interpretation and the diffraction patterns correspond to the spatial symmetry of the uranium sites. However, the measurements are rather insensitive to the presence of small moments (of order  $0.1\mu_B$ ) on the nickel atoms and we cannot exclude their existence.

Given this caveat, the moment on the  $n$ th uranium atom at position  $\mathbf{R}_n$  is given by

$$\mu_n = \mu_0 \hat{z} \cos(2\pi \mathbf{R}_n \cdot \mathbf{q} + \phi), \quad (1)$$

with  $\hat{z}$  a unit vector in the crystallographic  $c$  direction and  $\phi$  a phase angle.

Table I lists the integrated intensities of the magnetic Bragg peaks observed and calculated for this phase. Least-squares fitting of these intensities to moments given by Eq. (1), with form factors taken from Freeman *et al.*,<sup>7</sup> gives  $\mu_0 = (1.6 \pm 0.3)\mu_B$  with an  $R$  value of 3.4%.

The data indicate that the spin-density wave is in fact incommensurate, with  $q_z$  slightly less than  $\frac{3}{4}$ . At the temperature 110 K of the measurements discussed previously, the wave vector is only about 2.5 standard errors from the commensurate value of 0.75, but in fact there is a temperature dependence to  $q_z$ . This is shown in Fig. 3. The wave vector  $q_z$  has a maximum close to the commensurate value at a temperature of 107 K. This is about the temperature where the intensity of the Bragg peaks in this phase is a maximum. At higher and lower temperatures,  $q_z$  moves to values far from commensurability. Moreover, this temperature variation is seemingly continuous with no evidence of steplike behavior corresponding to locking in at various commensurate values.

The physical nature of the longitudinal spin-density wave is shown in Fig. 4 for  $q = \frac{3}{4}$ . A notable feature of the data is the absence of any reflections corresponding to harmonics of  $q$ . This shows that the spin-density wave is

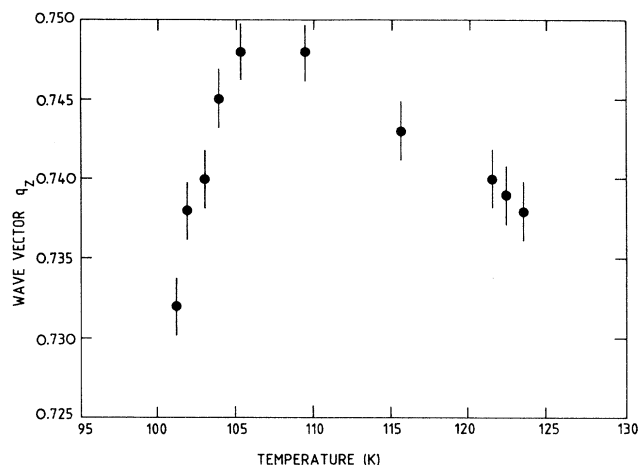


FIG. 3. Variation of the incommensurate wave vector as a function of temperature.

quite sinusoidal, though for the commensurate wave shown in Fig. 4 with  $q = \frac{3}{4}$  it is possible by adjusting the phase angle in Eq. (1) to produce a squared-off structure with the succession of ferromagnetic layers coming in pairs of up and down sheets.

TABLE I. Comparison of observed and calculated magnetic intensities for  $\text{UNi}_2\text{Si}_2$  at 11, 79, and 110 K.

$h$	$k$	$l$	11 K		$I_{\text{cal}}$ LSDW	$I_{\text{cal}}$ square	79 K		110 K	
			$I_{\text{obs}}$				$I_{\text{obs}}$	$I_{\text{cal}}$	$I_{\text{obs}}$	$I_{\text{cal}}$
1	0	0.000					3810	5088		
1	0	0.255							796	1085
1	0	0.333	1745	2463	2282					
1	0	1.667	1760	1571	1456					
1	0	0.745							694	658
1	0	2.000				2985	2682			
1	0	2.255							586	507
1	0	2.333	1488	1110	1028					
1	0	3.667	595	516	477					
1	0	3.745							291	214
1	0	4.000				915	855			
1	0	4.255							145	159
1	0	4.333	336	347	321					
2	0	0.667	2135	1488	1379					
2	0	0.745							807	644
2	0	1.000				3541	2891			
2	0	1.255							736	600
2	0	1.333	1833	1356	1256					
2	0	2.667	1087	959	889					
2	0	0.003							414	407
2	0	3.000				2403	1727			
2	0	3.255							345	340
2	0	3.333	690	756	700					
2	0	4.667	433	425	393					
2	0	4.745							163	178
		$R$ (%)		4.8	9.1		5.9			3.4
		magnetic moment ( $\mu_B$ )								
		$\mu_0$		$2.7 \pm 0.3$			$1.8 \pm 0.3$			$1.6 \pm 0.3$
		$\mu_z$		$1.0 \pm 0.3$						
		$ \mu_z $			$2.2 \pm 0.3$					

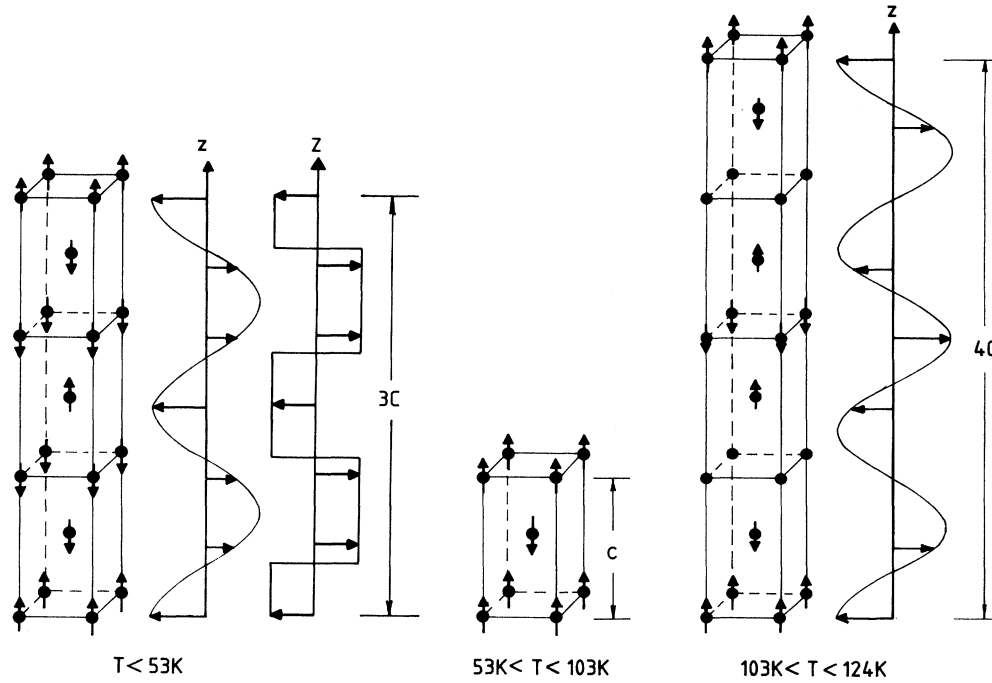


FIG. 4. Magnetic structure in the three phases. Two possible structures are shown for the low-temperature phase, on the left, LSDW, and on the right, square-wave modulated. The intermediate-temperature phase is a simple body-centered tetragonal antiferromagnet and the high-temperature phase is a LSDW.

### C. Intermediate-temperature phase

In this phase magnetic reflections are observed with indices such that

$$h + k + l = 2n + 1.$$

There are no magnetic reflections with  $h = k = 0$ . This pattern indicates a simply body-centered tetragonal antiferromagnet with the moments aligned along the  $c$  axis. The result of a least-squares fitting to the data at 80 K is given in Table I. The moment so obtained is  $(1.8 \pm 0.3)\mu_B$ .

### D. Low-temperature phase

The magnetic Bragg peaks in this phase are of the same type as those observed in the high-temperature phase but with  $q_z = 0.667 \pm 0.002$ . The value of  $q_z$  was the same for the two samples and did not change as the temperature was varied. Thus the low-temperature phase corresponds to a tripling of the unit cell along  $c$ . The absence of magnetic peaks of type  $(0,0,l)$  again indicates that the moments are aligned along the  $z$  direction. As was the case for the high-temperature phase, no peaks were observed corresponding to harmonics of  $q_z$ .

One possible interpretation of the data is that of a commensurate longitudinal spin-density wave along  $c$ . Least-squares fitting to this model gives a maximum sinusoidal moment of  $\mu_0 = (2.7 \pm 0.3)\mu_B$  with an  $R$  value of 4.8%. The observed and calculated intensities at 11 K are shown in Table I. The commensurate longitudinal

spin-density-wave structure that fits the data is shown in Fig. 4.

In addition, we searched for the ferromagnetic component of the moment suggested in Refs. 3 and 4. Such components give rise to magnetic Bragg peaks at the same position as the nuclear Bragg peaks, that is, at Bragg peaks with  $h + k + l$  even. The Bragg peak with the smallest structure factor of any within our experiment range is  $(1,0,1)$ ; we observed it to be weaker than any other nuclear Bragg peaks by a factor of 5. Thus the sensitivity to a ferromagnetic component in UNi<sub>2</sub>Si<sub>2</sub> is much higher at the  $(1,0,1)$  Bragg peak than at any other position. We observed that there is an increase of about 18% in the intensity of the  $(1,0,1)$  Bragg peak relative to both higher-temperature phases (Figure 5) for both samples. This buildup of intensity at  $(1,0,1)$  indicates a ferromagnetic component in the magnetization that corresponds to a magnetic moment of  $(1.0 \pm 0.3)\mu_B$ . Such an amount of moment should be just observable on the  $(0,0,l)$  nuclear peaks if the moment has an appreciable component in the  $x$ - $y$  plane. However, we did not observe any temperature change of the  $(0,0,2)$  Bragg peak within an error of  $0.3\mu_B$  (Fig. 5). Therefore, we believe that the ferromagnetic moment is along  $c$ . In contrast to Refs. 3 and 4, we observe no ferromagnetic moment in the temperature range  $53 < T < 103$  K, but only below 53 K.

The model corresponds to a magnetic moment on the  $n$ th uranium atom given by

$$\mu_n = [\mu_0 \cos(2\pi \mathbf{R}_n \cdot \mathbf{q}) + \mu_z] \hat{z}, \quad (2)$$

with  $\mu_0 = (2.7 \pm 0.3)\mu_B$  and  $\mu_z = (1.0 \pm 0.3)\mu_B$ .

This represents the best fit to our data. However, it is interesting to note that if  $\mu_0 = 4\mu_z$ , it is possible to construct a magnetic structure with the magnitude of all the uranium moments the same, so that the wave form is squared up. This could be achieved if

$$\mu_0 = 2.96\mu_B \text{ and } \mu_z = 0.74\mu_B .$$

These special values are within a standard error of our best-fit values and give  $R = 9.1\%$ . They are consistent with our experimental data and correspond to a magnetic cell with four moments of  $2.22\mu_B$  along the  $+z$  direction and two moments of  $2.22\mu_B$  along the  $-z$  direction. This structure is also shown in Fig. 4.

The squared-off wave picture of the low-temperature phase with  $\mu = (2.2 \pm 0.3)\mu_B$  is consistent with all our data.

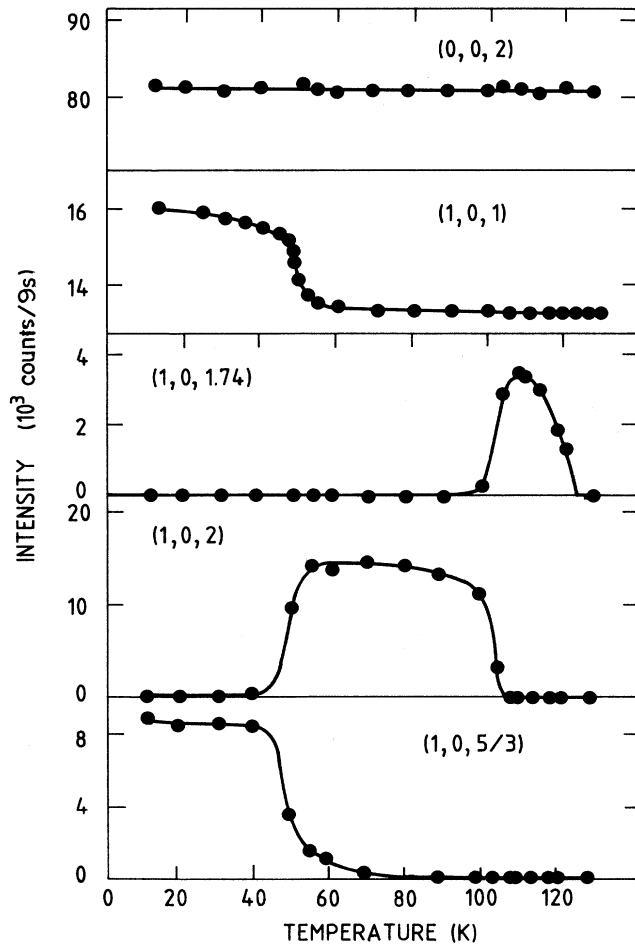


FIG. 5. Temperature dependence of the intensity of the  $(1,0, \frac{5}{3})$ ,  $(1,0,2)$ ,  $(1,0,1.74)$  magnetic Bragg peaks and of the  $(0,0,2)$  and  $(1,0,1)$  nuclear Bragg peaks. There are phase transitions at 53, 103, and 124 K.

### E. Magnetic phase transitions

The temperature dependences of the characteristic Bragg reflections on sample No. 1 are shown in Fig. 5. We can see that the low-temperature phase represented by the  $(1,0, \frac{5}{3})$  and  $(1,0,1)$  peaks is found below 53 K, the intermediate-temperature phase represented by the  $(1,0,2)$  peak is found between 53 and 103 K, and the high-temperature phase labeled by  $(1,0,1.74)$  exists between 103 and 124 K. The phase transitions occur at  $53 \pm 1$ ,  $103 \pm 1$ , and  $124 \pm 1$  K.

The study of those phase transitions has been carried out with both samples.

Above 124 K, as the system enters the paramagnetic phase from the incommensurate phase, critical scattering<sup>8</sup> is observed for  $\mathbf{Q} = (1,0,l)$  around  $l = 0.256$  and  $(h,0,0.256)$  around  $h = 1$  with sample No. 2. The evolution of the critical scattering as a function of temperature is shown in Figs. 6(a) and 6(b). The resolution is

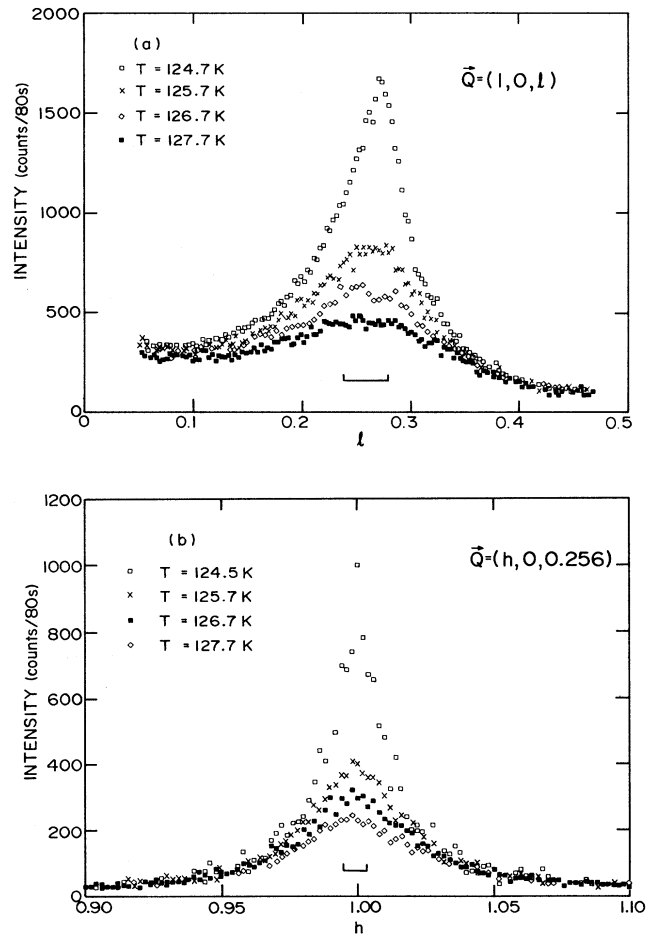


FIG. 6. Critical scattering along (a) the  $(1,0,l)$  and (b) the  $(h,0,0.256)$  directions at a series of temperatures just above the critical temperature. The resolution width is shown by the horizontal bar.

0.009±0.001 along  $a^*$  and 0.042±0.002 along  $c^*$ , from which the variation of the intrinsic width of the critical scattering may be determined.

The width of peaks in scans along  $c^*$  is about twice as large along  $a^*$  in reduced reciprocal lattice units, as shown in Fig. 6. However, in real space, the correlation length  $\xi$  (which is represented by the reciprocal of the width of peak) is essentially the same,  $\xi_c/\xi_a=0.94\pm0.1$ , in the two directions because the lattice parameter  $c$  is about twice  $a$ . Thus the critical region is isotropic. The correlation length  $\xi$  is 10.08 Å at 128.7 K and 19.31 Å at 124.7 K along  $c$ . We also observed that at all temperatures the critical scattering is centered about the position of the incommensurate magnetic Bragg peak at  $T_N$ ,  $Q=(1.000,0,0.265)$ .

The critical temperature  $T_c$  is estimated by extrapolating the integrated intensity of the (1,0,0.256) magnetic

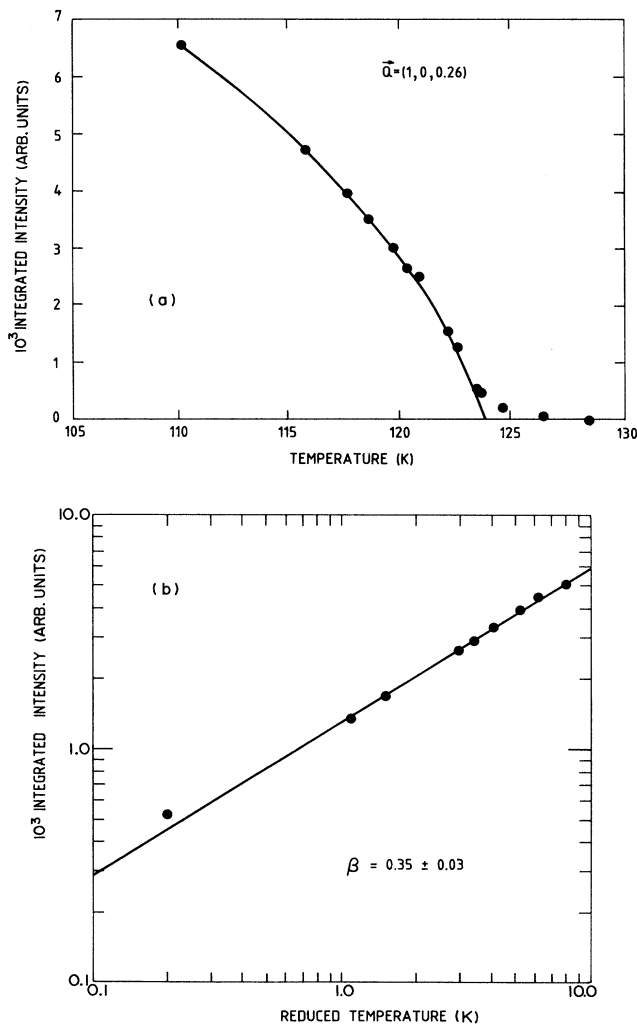


FIG. 7. (a) Temperature dependence of the integrated intensity of the (1,0,0.256) satellite in the critical regime below 124 K. (b) Log-log plot of integrated intensity vs reduced temperature. The slope gives a critical exponent  $\beta$  of  $0.35\pm0.03$ .

peak as a function of temperature in the critical regime [Fig. 7(a)]. Figure 7(b) shows a log-log plot of the integrated intensity against reduced temperature. The straight-line nature of the plot indicates that the intensity varies as a power law in reduced temperature, that is, as  $(T_c - T)^{2\beta}$ . The value of  $\beta$  is fitted to be  $0.35\pm0.03$ , which indicates that UNi<sub>2</sub>Si<sub>2</sub> is not a mean-field system, but instead is similar in behavior to a three-dimensional Ising or Heisenberg system.

The phase transition at 103 K which is between the incommensurate and antiferromagnetic phases behaves very differently from that at 124 K. The phase-transition region is about 4 K wide, which is rather narrow. In this region a rapid change of the order parameters represented by the intensity of (1,0,2) and (1,0,1.74) magnetic peaks was observed (Fig. 5). The width of those peaks remains resolution limited, and there is no temperature dependence of the observed width of the Bragg peaks to within an error of  $\pm 0.002$ . The incommensurate wave vector  $q_z$  decreases continuously when the temperature decreases (Fig. 3), but suddenly jumps to  $q_z=1$  when the antiferromagnetic phase is entered. No obvious hysteresis was observed. The above evidence shows that the phase transition is first order.

For the lowest-temperature phase transition, hysteresis effects were observed on the (1,0, $\frac{1}{3}$ ), (1,0,0), and (1,0,1) reflections with sample No. 2. Figure 8 shows the hysteresis of the (1,0,0) reflection with a 4° spread between increasing and decreasing temperatures. The full phase-transition region is about 20 K wide, and about half the sample changes phase in a central region 6 K wide. This is much broader than the transition at 103 K. Although the integrated intensity changes relatively slowly, it does not obey a power law. The position and width of the Bragg peaks are temperature independent. We conclude that this phase transition is also first order. Figure 8 also shows the behavior of sample No. 1 at the low-

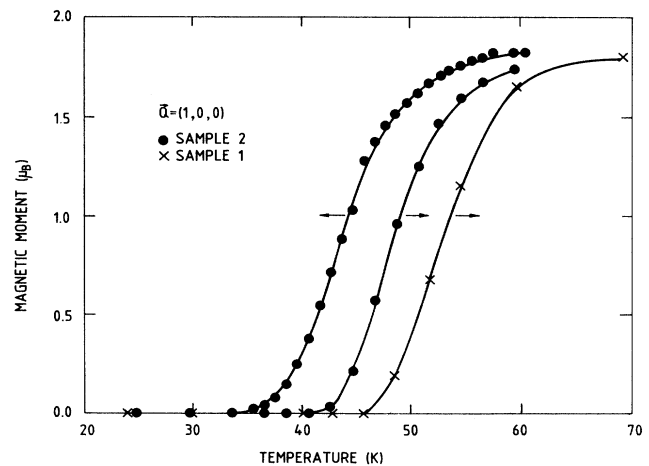


FIG. 8. Hysteresis of the (1,0,0) magnetic Bragg peak with sample No. 2. The plot also shows that samples Nos. 1 and 2 give different phase-transition temperatures. The arrows indicate the direction of the temperature variation.

temperature phase transition. It is notable that the two samples show transitions of similar width, but that the phase-transition temperature is different by 4 K. We have not been able to identify any differences between the two samples that can be connected to the difference of phase-transition temperature. A third crystal made by us and data given in the literature<sup>2</sup> give the same higher transition temperature that was observed for sample No. 1. This sample dependence of phase-transition temperature was not shown at the other two phase transitions, and in no other respect was the neutron scattering different between the two samples.

#### IV. DISCUSSION

Our neutron-diffraction data of  $\text{UNi}_2\text{Si}_2$  on single crystals agrees with the powder measurement by Chemicki, Leciejewicz, and Zygmunt except that, in addition, we observe a third long-range magnetic ordered phase in the temperature region 103–124 K. Close examination of the data of Chemicki, Leciejewicz, and Zygmunt shows evidence for the existence of the high-temperature phase in diffraction peaks that are attributed to short-range order.

The observation of oscillating moments with a net ferromagnetic component in the low-temperature phase was made in two different single crystals. This indicates that ferromagnetism is an intrinsic magnetic property of  $\text{UNi}_2\text{Si}_2$  at lower temperature, although the possibility of sample dependence of the value of ordered ferromagnetic moment exists since the moment in samples Nos. 1 and 2 was observed to be  $(0.9 \pm 0.3)\mu_B$  and  $(1.1 \pm 0.3)\mu_B$ , respectively. We do not find ferromagnetism below 98 K, as suggested in Ref. 3, but only below 53 K. Our study on phase transitions shows that a conventional isotropic critical scattering centered in the wave vector  $\mathbf{q}$  exists above 124 K. The critical phase transition from the incommensurate to the paramagnetic state has the critical exponent  $\beta = 0.35 \pm 0.03$ . The other two phase transitions are both first order, but the low-temperature phase transition shows hysteresis and sample dependence. So far,  $\text{UNi}_2\text{Si}_2$  has shown the most variety of magnetic ordering and phase-transition feature in series  $(\text{Ce,U})T_2X_2$  compounds.<sup>2,6,9,10</sup>

The different kinds of magnetic ordering of  $UT_2X_2$  have been explained by using the isotropic Ruderman-Kittel-Kasuya-Yosida model with a spherical Fermi surface.<sup>2,9,10</sup> A common theory is that the magnetism in  $(\text{Ce,U})T_2X_2$  arises from anisotropically indirect interac-

tion of the localized  $f$  electrons of the cerium or uranium through the hybridization with the itinerant conduction  $d$  electrons of transition metals. However, the assumption of a spherical Fermi surface seems unrealistic, and it is not possible in this model to explain the existence of three ordered structures at different temperatures. It is also possible to set up a model which gives a less localized character to the  $f$  electrons along the lines of the theory of spin-density waves.<sup>11,12</sup> This model explains the spin-density wave as arising from parallel areas of Fermi surface separated by a wave vector  $\mathbf{q}$ . There might be two such wave vectors corresponding to the commensurate and incommensurate structures corresponding to different areas of Fermi surfaces. At low temperatures there must be some mechanism to stabilize the commensurate structure, possibly arising from the large, and highly temperature-dependent, anisotropy energy in uranium compounds.

We note that all magnetic structures of  $\text{UNi}_2\text{Si}_2$  exhibit ferromagnetic sheets with moments perpendicular to the sheets. Any model of the magnetic structure would need to incorporate this feature of planar ferromagnetic coupling. Except for the ferromagnetic ordering, the three phases order antiferromagnetically, with moments either modulating from sheets to sheets or coupling up and down simply (Fig. 4). A possible theoretical framework to explain the  $\text{UNi}_2\text{Si}_2$  data may be the axial next-nearest-neighbor Ising (ANNNI) model since this model has Ising characteristics and can give rise to exotic structures of the type that we have observed. The spatially modulated phases, commensurate-commensurate phase transitions, and multiphase points in some rare-earth magnets like CeSb and USe-UAs have been described in terms of this model.<sup>6,13–15</sup> This model leads naturally to squared-up low-temperature structure<sup>6,15</sup> and would accommodate the squared-up structure that we have described as a possibility for the low-temperature phase.

#### ACKNOWLEDGMENTS

We thank Dr. T. E. Mason and Dr. S. Kim for aligning the samples. We also thank P. A. Moss, H. F. Nieman, T. L. Eve, and M. M. Potter (AECL) for technical assistance with the experiments at Chalk River. We would like to thank Dr. G. H. Lander for bringing the possibility of a squared-off model of the low-temperature phase to our attention. We are grateful to Y. B. Ning for the information on transport property of  $\text{UNi}_2\text{Si}_2$ . This research was supported by NSERC, CIDA, and U.S. Department of Energy Grant No. DE-AC02-76CH00016.

<sup>1</sup>R. A. Steeman, Ph.D. thesis, the University of Leiden, Netherlands, 1989; T. T. M. Palstra, A. A. Manowsky, G. J. Nieuwenhuys, and J. A. Mydosh, *J. Magn. Magn. Mater.* **54-57**, 435 (1986).

<sup>2</sup>L. Chelwicki, J. Leciejewicz, and A. Zygmunt, *J. Phys. Chem. Solids* **46**, 529 (1985).

<sup>3</sup>K. H. J. Buschow and D. B. DeMooij, *Philips J. Res.* **41**, 55 (1986).

<sup>4</sup>M. W. McElfresh, L. Rebelsky, M. S. Torikachvili, H. Borges, K. Reilly, S. Horn, and M. B. Maple, *J. Appl. Phys.* **67**, 5218 (1990).

<sup>5</sup>A. A. L. Dawson, W. R. Datars, J. D. Garrett, and F. S. Raza-vi, *J. Phys. Condens. Matter* **1**, 6817 (1989).

<sup>6</sup>B. H. Grier, J. M. Lawrence, V. Murgai, and R. D. Parks, *Phys. Rev. B* **29**, 2664 (1984).

<sup>7</sup>A. J. Freeman, J. P. Desclaux, G. H. Lander, and J. Faber, Jr.,

- Phys. Rev. B **13**, 1168 (1976).
- <sup>8</sup>M. F. Collins, *Magnetic Critical Scattering* (Oxford University Press, New York, 1989).
- <sup>9</sup>A. Szytula, S. Siek, J. Leciejewicz, A. Zygmunt, and Z. Ban, J. Phys. Chem. Solids **49**, 1113 (1988).
- <sup>10</sup>H. Ptasiwicz-Bak, J. Leciejewicz, and A. Zygmunt, J. Phys. F **11**, 1225 (1981).
- <sup>11</sup>E. Fawcett, Rev. Mod. Phys. **80**, 209 (1988).
- <sup>12</sup>C. Herring, in *Magnetism IV*, edited by G. T. Rado and H. Suhl (Academic, New York, 1966), p. 1.
- <sup>13</sup>P. Bak and J. Von Boehm, Phys. Rev. B **21**, 5297 (1980).
- <sup>14</sup>M. E. Fisher, J. Appl. Phys. **52**, 2014 (1981).
- <sup>15</sup>J. Rossat-Mignod, in *Methods of Experimental Physics 23(C), Neutron Scattering*, edited by K. Sköld and D. L. Price (Academic, Orlando, FL, 1987), p. 143.